Tightly-Confined and Long Z-Cut Lithium Niobate Waveguide with Ultralow-Loss

Citation for the original published paper (version of record):
Gao, Y., Sun, Y., Rebolledo Salgado, I. et al (2025). Tightly-Confined and Long Z-Cut Lithium Niobate Waveguide with Ultralow-Loss. Laser and Photonics Reviews, In Press.
http://dx.doi.org/10.1002/lpor.202500042

(article starts on next page)

Tightly-Confined and Long Z-Cut Lithium Niobate Waveguide with Ultralow-Loss

*Yan Gao, Yi Sun, Israel Rebolledo-Salgado, Raphaël Van Laer, Victor Torres-Company, and Jochen Schröder**

Lithium niobate (LN) is a promising material for complex photonic-electronic circuits with wide applications in fields like data communications, sensing, optical computation, and quantum optics. There is a great step toward LN photonic integrated circuits (PICs) with the development of dry etching for low-loss LN on insulator (LNOI) waveguides. However, the versatility of the LN waveguide platform for applications like χ^3 nonlinear devices and passive phase sensitive components, has not been fully utilized. Two significant challenges are the difficulty of making highly confined ultralow-loss waveguides and overcoming the strong material birefringence. Here a fabrication technology is developed for an ultralow-loss, tightly-confined, dispersion-engineered LN waveguide. An ultra-low propagation loss of 5.8 dB/m is demonstrated in a decimeter-long LN spiral waveguide. This study is focused on Z-cut LN waveguides with TE mode to avoid the material birefringence. Aiming for χ^3 nonlinear applications, it is demonstrated that the first all normal-dispersion (ANDi) based coherent octave-spanning supercontinuum frequency comb in integrated LN waveguide. This ultralow-loss Z-cut LN long waveguide might be useful in on-chip narrow linewidth lasers, optical delay lines, and parametric amplifiers.

1. Introduction

Photonic integrated circuits[1] (PICs) enable on-chip light generation, manipulation, and detection. Via integration and miniaturization, PICs show great potential for realizing low-cost and scalable optical systems in fields like data communication, bio-chemical sensing and optical computation. In recent decades, different material platforms have been investigated, including silicon (Si),[2] indium phosphide (InP),[3] silicon nitride (SiN_x),[4–7] aluminum gallium arsenide (AlGaAs),[8,9] aluminium nitride (AlN),[10] silicon carbide (SiC),[11] and lithium niobate (LN).[12–15]

Recently, LN has attracted large research interest due to its unique properties that can simultaneously provide electro-optic (EO), nonlinear and acousto-optic effects. Moreover, it exhibits a broad optical transparency window, a high refractive-index-contrast, and ultra-low material losses.[16–19] Photonic applications in LN such as low drive voltage high-speed EO modulators,[20,21] Kerr and EO frequency combs,[13,22] ultra-efficient frequency converters,[23,24] squeezed light sources,[25] photon pair sources[26] and parametric optical oscillators[27,28] have been demonstrated.

Long waveguides with ultralow losses are crucial for a host of chip-scale applications, such as narrow linewidth lasers,[29] optical delay lines,[30–32] and nonlinear optical processes like parametric amplifiers.[33,34] Such waveguides have been built in dielectric materials like Si_3N_4[33,35,36] and SiO_2[30] with losses in the dB/m regime. For LNOI, however, it is a bigger challenge and has so far remained elusive because of the waveguide fabrication difficulty and strong material birefringence.

In this work, we leverage recent advances in fully etched LN waveguides[15] and further develop the methodology to achieve ultra-low loss strongly confined Z-cut spiral-waveguides. We demonstrates the first ultra-low loss (5.8 dB/m) long waveguide in LN with propagation loss approaching the record-low value (2.7 dB/m) that extracted from X-cut micro-racetracks reported in [12]. The ultra-low loss combined with a Z-cut configuration allows us to reach decimeter long interaction lengths, enabling octave-spanning supercontinuum in an all-normal-dispersion LN waveguide for the first time, to the best of our knowledge.

2. Z-cut LN long waveguide platform

LN is a well-known anisotropic material, in which the nonlinear and EO coefficients vary largely in different directions. To take advantage of the largest EO (r_{33}) or second order nonlinear coefficient (d_{33}), most work has focused on the TE polarization in X-cut LN waveguides. However, the strong birefringence limits

Y. Gao, Y. Sun, I. Rebolledo-Salgado, R. Van Laer, V. Torres-Company, J. Schröder
Department Of Microtechnology And Nanoscience (Mc2)
Chalmers University of Technology
Göteborg SE-412 96, Sweden
E-mail: jochen.schroeder@chalmers.se

The ORCID identification number(s) for the author(s) of this article can be found under https://doi.org/10.1002/lpor.202500042

DOI: 10.1002/lpor.202500042

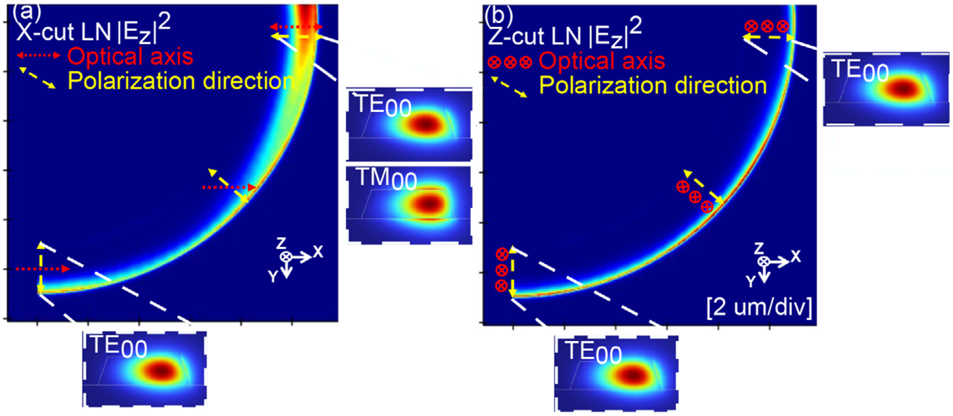

Figure 1. a) The simulated optical field (Z component) distribution in a X-cut LN bent waveguide. The input is TE_{00} mode. After propagation, partial energy transferred to TM_{00} mode due to the index anisotropy. b) The same field profile but in a Z-cut LN bent waveguide, where there is no energy transfer from TE_{00} to TM_{00}.

the waveguide layout to a single direction. Such configuration will also make the in-plane optical index to experience large changes ($\Delta n = 0.08$) with waveguide direction because of the birefringence. The resulting direction-dependent index will cause serious intermode-crosstalk[37] even in a single-moded bent waveguide. The index anisotropy will increase the design complexity and special consideration is required for phase sensitive or dispersion components such as arrayed waveguide grating (AWG).[38] As showed in **Figure 1a**, for an X-cut bent waveguide, the light mode will be distorted by the index

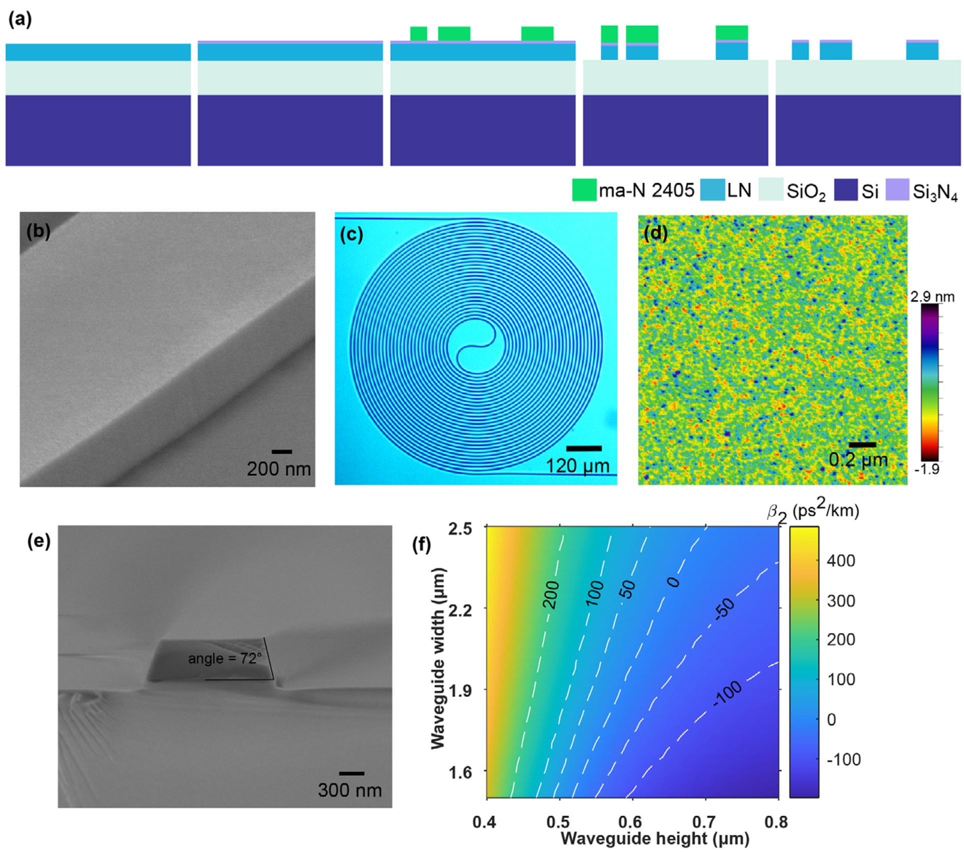

Figure 2. a) Fabrication flow chart for fully etched LN waveguide. b) SEM image of LN ring resonators and e) zoomed in SEM image for waveguide sidewall, the figure was post-colored to highlight LN waveguide. c) Top view microscope image for a spiral waveguide in one writing field. d) AFM measurement for the surface roughness of Si_3N_4 sputtered on LN, the measured surface RMS roughness is 0.5 nm. f) Simulated dispersion (FEM, COMSOL multiphysics) of the fully etched LN waveguide with the bending radius of 200 µm.

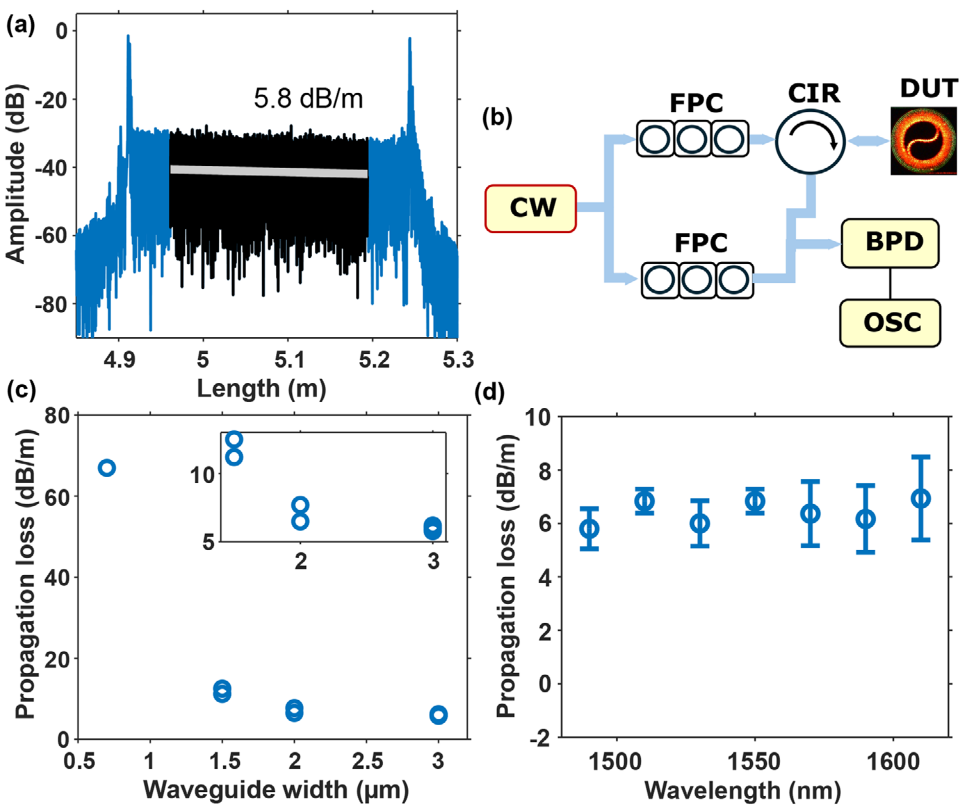

Figure 3. a) OFDR measurement results for a 15 cm long waveguide. b) Experimental setup. c) Measured losses with different waveguide width. d) Measured losses with different wavelength.

anisotropy, and energy of the input TE_{00} mode will transfer to the TM_{00} mode. However, the mode will maintain the same energy when propagating in a Z-cut bent waveguide.

Below we give a detailed explanation of our fabrication process to obtain ultra-low loss tightly-confined LN waveguides.

The samples for the waveguide fabrication are diced from a 4 inch commercial LN wafer (NANOLN). The wafer includes 600 nm thin film LN on top, 525 µm thick silicon substrate at the bottom, and 4.7 µm thermally oxidized SiO_2 in between. **Figure** 2a shows the fabrication flow. The sample is first prepared via solvent cleaning (acetone, IPA) and then via standard cleaning (SC1, 29% NH_3: 30% H_2O_2: $H_2O = 1{:}1{:}5$). To minimize the effect from the SC1 solution on the LN, we limit the SC1 time to 2 minutes only. The sample is then sent to the vacuum sputtering tool (FHR, MS150), and around 5 nm Si_3N_4 is deposited on the top of the LN, to promote the adhesion between LN and resist. Using atomic force microscopy (AFM), we measure the surface roughness of the sample after Si_3N_4 deposition, and the measured root mean square roughness (RMS) is 0.5 nm. The surface roughness is slightly increased compared to the pure LN surface (around 0.3 nm). However, the increased top surface roughness does not contribute significantly to the waveguide losses according to our measurement results, and we believe that the losses are still mainly governed by the waveguide sidewall roughness.

Negative tone electro-beam lithography (EBL) resist ma-N 2405 is adopted for its high resolution, dry etch resistance, and more importantly, good thermal stability. The pattern is first defined on the resist via 100-kV EBL system (Raith, EBPG 5200), in which multipass exposure is used to reduce sidewall roughness. A beam step size (BSS) of 3 nm was chosen and the delivered doses were 230 µC/cm^2. The dose will influence the sidewall roughness and should be optimized for different fabrication flows. Moreover, resistance to ion milling is important because of the pure physical etching process and the deep etching depth here. We found that a larger dose tends to give better resistance during dry etching. As a result, the dose should be optimized by considering both the roughness and the resist resistance.

After exposure and development, the sample is then dry-etched via reactive ion beam etching (IBE, Oxford Ionfab 300 Plus) with only Ar^+ plasma. The Ar^+ gas flow used for the plasma generation is 6 sccm. A higher concentration of Ar^+ plasma will lead to a higher etching rate. The generated Ar^+ plasma will be accelerated via electric field and directly bombards the LN surface. The pure physical etching process results in poor selectivity (around 1.4). The measured etching rate of LN is around 14 nm/min and 45 min is required to achieve slightly overetching for 600 nm LN. During the etching process, especially for our fully etched waveguides, we observe strong thermal accumulation that can cause local burning of the resist even with helium cooling. We therefore adopt a strategy to keep the temperature at a certain low level: 1) Choose a thermally stable resist (ma-N 2405); 2) Use thermal release tape between sample and carrier wafer; 3) Perform multiple etching steps to allow cooling of the sample. The sidewall angle

Table 1. Summary of propagation losses (quality factor) of MRRs and long waveguide for different waveguide structures.

LN cut type	H_{etch}/H_{total} (nm)	Bending radius (µm)	Width (µm)	Intrinsic Q	Optical loss (dB/m)	Year
X-cut	350/600	80, MRR	0.8–2.4	$1.5\text{-}4 \times 10^6$	27.3–10.2[a]	2017[12]
	350/600	Race-track	2.4	10×10^6	2.7[b]	2017[12]
X-cut	700/700	20–180, MRR	3	3.5×10^6[e]	11.6[a]	2023[41]
	700/700	240, MRR	3	10×10^6	4	2023[41]
Z-cut	600/600	40, MRR	2.1	4.9×10^6[e]	8.4[a]	2023[15]
	600/600	20, MRR	2.1	3.8×10^6[e]	10.8[a]	2023[15]
X-cut/Si_3N_4	950[c]	200, MRR	2	3×10^6[e]	12.75	2022[42]
	950[c]	400, MRR	2	4.5×10^6[e]	8.5	2022[42]
X-cut	300/600	140, MRR	2.4	5×10^6[e]	8.2[a]	2022[43]
X-cut	320/500	100, MRR	0.9	1.8×10^6[e]	22.7[a]	This work
Z-cut	400/600	100, MRR	1.0	2.0×10^6[e]	20.5[a]	This work
Z-cut	600/600	long waveguide	0.7	/	67.0[d]	This work
	600/600	long waveguide	1.5	/	11.2[d]	This work
	600/600	long waveguide	2.0	/	6.5[d]	This work
	600/600	long waveguide	3.0	/	5.8[d]	This work

[a] Estimated optical loss from the Q-factor by assuming a group index of 2.28. [b] Extrated optical loss in the straight section of a long micro-racetrack resonator. [c] The hybrid integration between LN and Si_3N_4, and the 950 is the height of the Si_3N_4 waveguide. [d] Average loss. [e] Statistical Q.

of the waveguides is estimated to be around 72 degrees which is due to the lateral etching of resist during the physical etching. Finally, the sample is sent for another run of solvent and standard cleaning to remove the remaining resist and by-products.

3. Losses Characterization

We fabricated long spiral waveguides to characterize the propagation losses. Figure 2c shows a microscope image for a fabricated spiral waveguide.

The spiral shape reduces the footprint for the entire device. We minimize stiching errors (and thus extra losses), by intentionally fitting each spiral unit into a single writing file (1 × 1 mm^2).[33] Each spiral unit includes two centrosymmetric Archimedean spirals and an S-bend to connect them. Since any sharp change in curvature of a waveguide will introduce radiation loss and intermode coupling between different transverse modes, a smoothly varying S-bend is needed to connect the two Archimedean spirals. We consider a curves family in which the curvature is given in terms of a cubic polynomial of arc length 's':[39,40]

$$\kappa(s) = a_0 + a_1 s + a_2 s^2 + a_3 s^3 \tag{1}$$

The coefficients a_0, a_1, a_2, a_3 can be solved by using the boundary conditions at the initial and final connection points with physical position, the tangent, the curvature and the change of the curvature. Figure 4a shows mode profile for the s-bend from a numerical simulation (Ansys, FDTD), the input TE_{00} mode could be smoothly transferred to the output port without significant mode coupling to high-order modes, and the optical loss for such a s-bend is neglectable as shown in Figure 4b.

Optical frequency-domain reflectometry (OFDR) based on Rayleigh scattering[33,44] is used to characterize the propagation losses of our waveguide. The measurement setup is shown in Figure 3b. It includes a sweeping CW laser, fiber delay path, and a photo-detector. By applying an inverse-Fourier transform of the temporal distribution of the reflected power from the spiral waveguide, the reflected power as a function of time delay/length

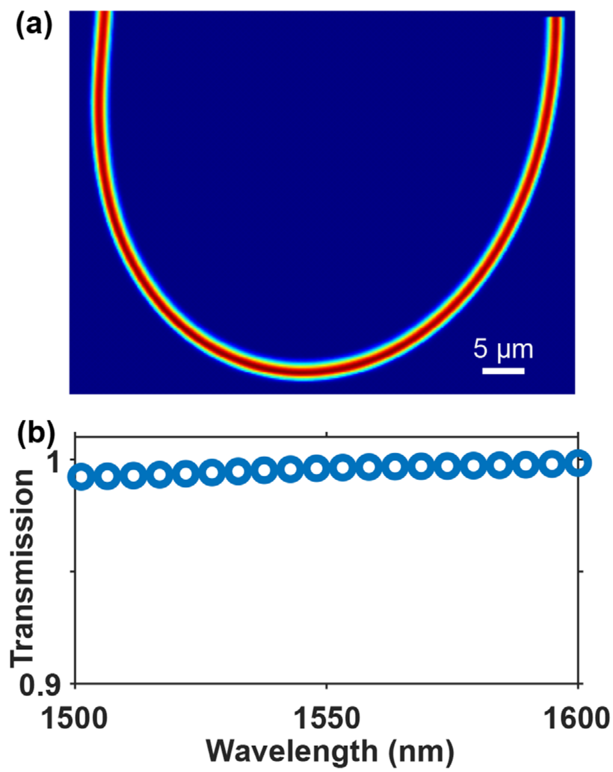

Figure 4. a) The simulated optical field distribution in the half s-bend in a spiral, and b) the corresponding simulated transmission for the s-bend. The sidewall angle of the waveguide is not considered and a vertical angle is assumed in the simulation.

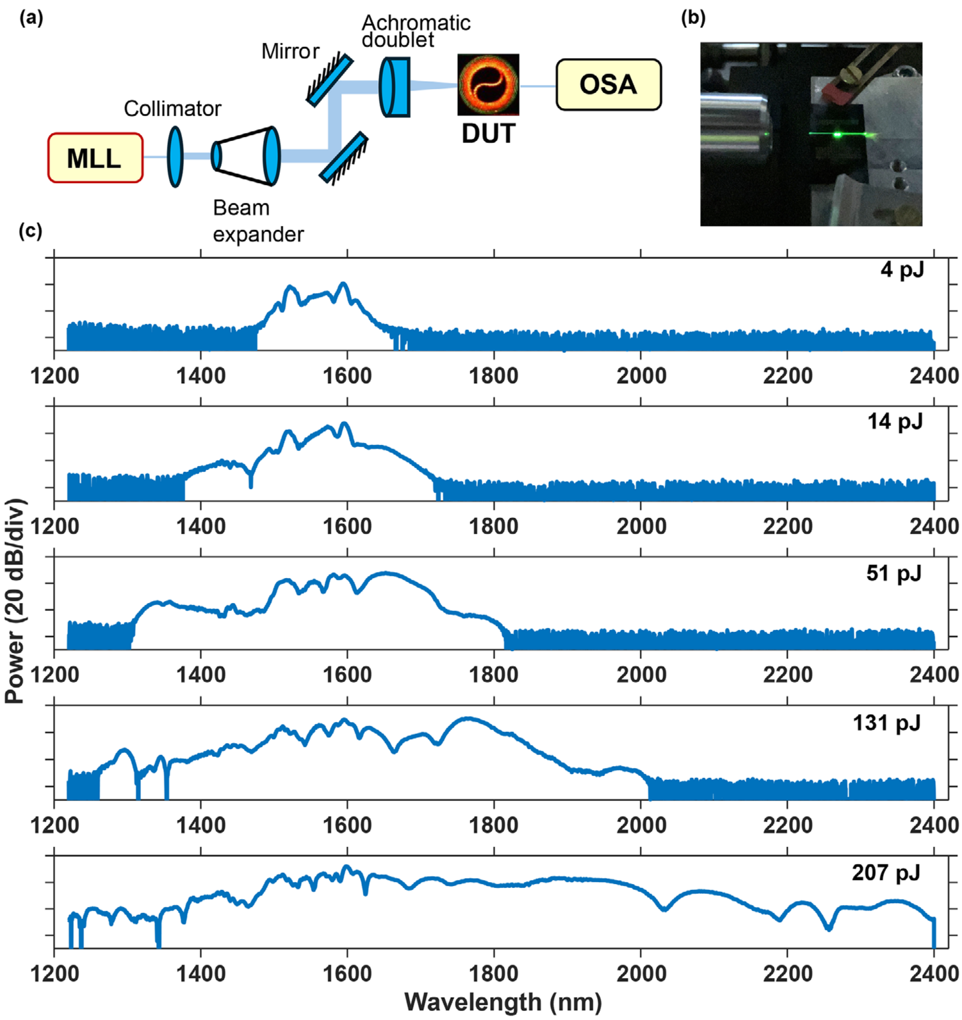

Figure 5. a) Experimental setup for supercontinuum generation, the light is free-space coupled onto the chips. b) Picture for the measured setup. c) The measured spectrum when pump with different power.

can be determined and the propagation loss can be obtained by linear fitting. Figure 3a shows OFDR measurement result for a 15 cm long spiral waveguide with the lowest loss, and the measured loss is 5.8 dB/m. To the best of our knowledge, this constitutes the lowest loss measured directly in a decimeter-long LN waveguide. The measured loss corresponds to a mean value over the wavelength range of 1480–1620 nm. To further characterize the loss at different wavelengths, we considered 3 different devices with the same waveguide width of 3 µm and processed the data to obtain the loss at different wavelengths. The measured results are consistent with each other, and all devices exhibit a similar loss over the full measured wavelength range. Propagation losses with different waveguide widths from 700 nm to 3 µm were also measured and are shown in Figure 3c. The statistical characterization of losses in different waveguide widths was constrained by practical limitations in our academic-grade EBL system, where fabricating a large number of long waveguides proves challenging. The propagation loss is around 0.67 dB/cm in the single mode regime (700 nm) and decreases dramatically for multi-mode waveguides, as the mode will be more confined and located in the central region and experiences less interaction with the sidewall roughness. Ultra-low propagation losses down to a few dB/m has been demonstrated here for reasonable widths multi-mode waveguides.

Table 1 summarizes the state-of-the-art achievements for high-Q LN resonators, providing a detailed compassion with our low-loss long waveguide. Given that waveguide loss exhibits strong geometric dependence and meaningful quality comparison requires explicit dimensional information, we meticulously list the exact waveguide geometries (width/height/etch depth) and resonator dimensions in the table. As shown in Table 1, our work demonstrates the first ultra-low loss long waveguide in LN with propagation loss approaching the record-low value (2.7 dB/m) that extracted from X-cut micro-racetracks reported in.[12] Notably, our LN fabrication method is directly applicable to X-cut LN substrates. To validate this capability, we present measurement results for partially etched micro-ring resonators (MRRs) fabricated on both X-cut and Z-cut LN platforms. Remarkably, both configurations achieve intrinsic Q-factors approaching 2 million despite employing narrow waveguide widths (900 nm for X-cut, 1000 nm for Z-cut). This performance represents a significant advancement in low-loss LN photonic circuits.

4. Nonlinear applications based on χ^3

We study supercontinuum generation in an all-normal dispersion LN waveguide with geometry of $2.7 \times 0.6\ \mu m^2$ and length of 30 cm. The device used for the experiment includes 6 cascaded spiral units with around 5 cm length for each. Considering the high light confinement of our waveguide, a denser spiral design is possible (by decreasing the waveguide gap and the minimum bending radius), to improve the total length (for example, to achieve a meter-long waveguide), while maintaining an ultra-low propagation loss. The measurement setup is shown in **Figure** 5a. A 50 femtosecond mode lock laser (MLL) with a center wavelength of 1560 nm and repetition rate of 250 MHz is used to pump the device. The laser beam is first collimated and expanded to obtain a diffraction limited spot size. The mirrors are used to align the height of the beam and the achromatic doublet is used to focus the beam onto the waveguide facet. A half-wave plate is used to tune the beam polarization to couple the light into the waveguide's TE mode. The estimated input coupling loss is around 10 dB. We attribute the large coupling loss to the suboptimal overlap between waveguide and the focused beam spot. The light is coupled from the waveguide to a lensed fiber with beam diameter of 2.5 μm. After the lensed fiber, we use a single mode fiber connected to an OSA (wavelength range of 1200–2400 nm) to measure the spectrum.

We carried out measurements with varying optical input power using a series of free space optical density filters. As shown in Figure 5c, the spectrum broadens when the on-chip pump power is increased. The spectrum reaches one octave spanning at a pump pulse energy of around 207 pJ. Unlike anomalous dispersion supercontinuum, the coherence of the broadened pulse in the ANDi waveguides is maintained over relatively long propagation lengths and high energy pulses.[45–47] The maximum spectrum bandwidth is limited by the available MLL power and the suboptimal coupling losses from free space to chip.

5. Conclusion

In conclusion, a LN waveguide fabrication technology has been developed to realize a fully-etched strip LN waveguide with advantages for simultaneously achieving ultra-low propagation losses, strong light confinement and dispersion engineering. We focused on Z-cut LN to avoid the material anisotropy, but the fabrication technology is not limited to only Z-cut LN. Utilizing the developed LN waveguide, we showed an ultralow-loss down to a few dB/m by using a 15-cm long spiral waveguide. Utilizing the long waveguide, we demonstrate an octave-spanning supercontinuum in the all normal-dispersion regime. Our ultralow loss long LN waveguide is desirable for chip-scale narrow linewidth lasers,[29] low loss optical delay lines,[30–32] and parametric amplification.[33,34] In addition, combined with periodic poling, the ultralow loss long waveguide could also be used for χ^2 nonlinear applications where a long interaction length is required. A Z-cut LN modulator in a spiral long waveguide will also be attractive to release layout restrictions in X-cut configurations and further reduce the drive voltage. Considered the high light confinement of the waveguide platform, it will also be useful for densely integrated optical components, such as large-scale optical switching arrays,[48] integrated photonic LiDAR,[49] and optical artificial intelligence.[50]

Acknowledgements

The authors thank cleanroom staff from Myfab at Chalmers Nanofabrication Laboratory for discussion and training. Funding: Swedish Research council (VR-2017-05157, VR-2021-04241).

Conflict of Interest

The authors declare no conflict of interest.

Data Availability Statement

The data that support the findings of this study are available in zenodo at https://doi.org/10.5281/zenodo.14606023, reference number [51].

Keywords

integrated photonics, lithium niobate, long waveguide, nonlinear optics

Received: January 7, 2025
Revised: June 2, 2025
Published online:

[1] T. David, Z. Aaron, B. John E, T. Komljenovic, R. Graham T, V. Laurent, M.-M. Delphine, C. Eric, V. Léopold, F. Jean-Marc, H. Jean-Michel, S. Jens H, X. Dan-Xia, B. Frédéric, O. Peter, M. Goran Z, *J. Opt.* **2016**, *18*, 073003.
[2] B. Jalali, S. Fathpour, *J. Light. Technol.* **2006**, *24*, 4600.
[3] M. Smit, K. Williams, J. Van Der Tol, *APL Photonics* **2019**, *4*, 5.
[4] Y. Xuan, Y. Liu, L. T. Varghese, A. J. Metcalf, X. Xue, P.-H. Wang, K. Han, J. A. Jaramillo-Villegas, A. Al Noman, C. Wang, S. Kim, M. Teng, Y. J. Lee, B. Niu, L. Fan, J. Wang, D. E. Leaird, A. M. Weiner, M. Qi, *Optica* **2016**, *3*, 1171.
[5] X. Ji, F. A. Barbosa, S. P. Roberts, A. Dutt, J. Cardenas, Y. Okawachi, A. Bryant, A. L. Gaeta, M. Lipson, *Optica* **2017**, *4*, 619.
[6] J. Liu, A. S. Raja, M. Karpov, B. Ghadiani, M. H. Pfeiffer, B. Du, N. J. Engelsen, H. Guo, M. Zervas, T. J. Kippenberg, *Optica* **2018**, *5*, 1347.
[7] Z. Ye, K. Twayana, P. A. Andrekson, V. Torres-Company, *Opt. Express* **2019**, *27*, 35719.
[8] M. Pu, L. Ottaviano, E. Semenova, K. Yvind, *Optica* **2016**, *3*, 823.
[9] L. Chang, W. Xie, H. Shu, Q.-F. Yang, B. Shen, A. Boes, J. D. Peters, W. Jin, C. Xiang, S. Liu, et al., *Nat. Commun.* **2020**, *11*, 1331.
[10] H. Jung, K. Y. Fong, C. Xiong, H. X. Tang, *Opt. Lett.* **2013**, *39*, 84.
[11] M. A. Guidry, K. Y. Yang, D. M. Lukin, A. Markosyan, J. Yang, M. M. Fejer, J. Vučković, *Optica* **2020**, *7*, 1139.
[12] M. Zhang, C. Wang, R. Cheng, A. Shams-Ansari, M. Lončar, *Optica* **2017**, *4*, 1536.
[13] Y. He, Q.-F. Yang, J. Ling, R. Luo, H. Liang, M. Li, B. Shen, H. Wang, K. J. Vahala, Q. Lin, *Optica* **2019**, *6*, 1138.
[14] Z. Gong, X. Liu, Y. Xu, M. Xu, J. B. Surya, J. Lu, A. Bruch, C. Zou, H. X. Tang, *Opt. Lett.* **2019**, *44*, 3182.

[15] Y. Gao, F. Lei, M. Girardi, Z. Ye, R. Van Laer, V. Torres-Company, J. Schröder, *Opt. Lett.* **2023**, *48*, 3949.
[16] D. Zhu, L. Shao, M. Yu, R. Cheng, B. Desiatov, C. Xin, Y. Hu, J. Holzgrafe, S. Ghosh, A. Shams-Ansari, E. Puma, N. Sinclair, C. Reimer, M. Zhang, M. Lončar, *Adv. Opt. Photonics* **2021**, *13*, 242.
[17] Y. Qi, Y. Li, *Nanophotonics* **2020**, *9*, 1287.
[18] A. Honardoost, K. Abdelsalam, S. Fathpour, *Laser Photonics Rev.* **2020**, *14*, 2000088.
[19] R. Weis, T. Gaylord, *Appl. Phys. A* **1985**, *37*, 191.
[20] C. Wang, M. Zhang, X. Chen, M. Bertrand, A. Shams-Ansari, S. Chandrasekhar, P. Winzer, M. Lončar, *Nature* **2018**, *562*, 101.
[21] M. He, M. Xu, Y. Ren, J. Jian, Z. Ruan, Y. Xu, S. Gao, S. Sun, X. Wen, L. Zhou, L. Liu, C. Guo, H. Chen, S. Yu, L. Liu, X. Cai, *Nat. Photonics* **2019**, *13*, 359.
[22] M. Zhang, B. Buscaino, C. Wang, A. Shams-Ansari, C. Reimer, R. Zhu, J. M. Kahn, M. Lončar, *Nature* **2019**, *568*, 373.
[23] J. Lu, J. B. Surya, X. Liu, A. W. Bruch, Z. Gong, Y. Xu, H. X. Tang, *Optica* **2019**, *6*, 1455.
[24] J.-Y. Chen, Z.-H. Ma, Y. M. Sua, Z. Li, C. Tang, Y.-P. Huang, *Optica* **2019**, *6*, 1244.
[25] R. Nehra, R. Sekine, L. Ledezma, Q. Guo, R. M. Gray, A. Roy, A. Marandi, *arXiv preprint arXiv:2201.06768* **2022**.
[26] J. Zhao, C. Ma, M. Rüsing, S. Mookherjea, *Phys. Rev. Lett.* **2020**, *124*, 163603.
[27] J. Lu, A. Al Sayem, Z. Gong, J. B. Surya, C.-L. Zou, H. X. Tang, *Optica* **2021**, *8*, 539.
[28] T. P. McKenna, H. S. Stokowski, V. Ansari, J. Mishra, M. Jankowski, C. J. Sarabalis, J. F. Herrmann, C. Langrock, M. M. Fejer, A. H. Safavi-Naeini, *Nat. Commun.* **2022**, *13*, 4532.
[29] C. Xiang, W. Jin, J. Guo, J. D. Peters, M. Kennedy, J. Selvidge, P. A. Morton, J. E. Bowers, *Optica* **2020**, *7*, 20.
[30] H. Lee, T. Chen, J. Li, O. Painter, K. J. Vahala, *Nat. Commun.* **2012**, *3*, 867.
[31] S. Hong, L. Zhang, Y. Wang, M. Zhang, Y. Xie, D. Dai, *Photonics Res.* **2021**, *10*, 1.
[32] X. Ji, X. Yao, Y. Gan, A. Mohanty, M. A. Tadayon, C. P. Hendon, M. Lipson, *APL Photonics* **2019**, *4*, 9.
[33] Z. Ye, P. Zhao, K. Twayana, M. Karlsson, V. Torres-Company, P. A. Andrekson, *Sci. Adv.* **2021**, *7*, eabi8150.
[34] T. Kazama, T. Umeki, S. Shimizu, T. Kashiwazaki, K. Enbutsu, R. Kasahara, Y. Miyamoto, K. Watanabe, *Opt. Express* **2021**, *29*, 28824.
[35] J. F. Bauters, M. J. Heck, D. John, D. Dai, M.-C. Tien, J. S. Barton, A. Leinse, R. G. Heideman, D. J. Blumenthal, J. E. Bowers, *Optics express* **2011**, *19*, 3163.
[36] J. Liu, G. Huang, R. N. Wang, J. He, A. S. Raja, T. Liu, N. J. Engelsen, T. J. Kippenberg, *Nat. Commun.* **2021**, *12*, 2236.
[37] B. Pan, Y. Tan, P. Chen, L. Liu, Y. Shi, D. Dai, *J. Light. Technol.* **2020**, *39*, 1770.
[38] J. Yi, C. Guo, Z. Ruan, G. Chen, H. Wei, L. Lu, S. Gong, X. Pan, X. Shen, X. Guan, et al., *Light Sci. Appl.* **2024**, *13*, 147.
[39] T. Chen, H. Lee, J. Li, K. J. Vahala, *Opt. Express* **2012**, *20*, 22819.
[40] Z. Ye, F. Lei, K. Twayana, M. Girardi, P. A. Andrekson, V. Torres-Company, *Laser Photonics Rev.* **2022**, *16*, 2100147.
[41] Z. Li, R. N. Wang, G. Lihachev, J. Zhang, Z. Tan, M. Churaev, N. Kuznetsov, A. Siddharth, M. J. Bereyhi, J. Riemensberger, et al., *Nat. Commun.* **2023**, *14*, 4856.
[42] M. Churaev, R. N. Wang, A. Riedhauser, V. Snigirev, T. Blésin, C. Möhl, M. H. Anderson, A. Siddharth, Y. Popoff, U. Drechsler, et al., *Nat. Commun.* **2023**, *14*, 3499.
[43] A. Shams-Ansari, G. Huang, L. He, Z. Li, J. Holzgrafe, M. Jankowski, M. Churaev, P. Kharel, R. Cheng, D. Zhu, N. Sinclair, B. Desiatov, T. Kippenberg, M. Lončar, *APL Photonics* **2022**, *7*, 081301.
[44] C. Liang, Q. Bai, M. Yan, Y. Wang, H. Zhang, B. Jin, *IEEE Access* **2021**, *9*, 41647.
[45] C. Finot, B. Kibler, L. Provost, S. Wabnitz, *JOSA B* **2008**, *25*, 1938.
[46] J. M. Dudley, S. Coen, *Opt. Lett.* **2002**, *27*, 1180.
[47] I. Rebolledo-Salgado, Z. Ye, S. Christensen, F. Lei, K. Twayana, J. Schröder, M. Zelan, V. Torres-Company, *Opt. Express* **2022**, *30*, 8641.
[48] T. J. Seok, K. Kwon, J. Henriksson, J. Luo, M. C. Wu, *Optica* **2019**, *6*, 490.
[49] X. Zhang, K. Kwon, J. Henriksson, J. Luo, M. C. Wu, *Nature* **2022**, *603*, 253.
[50] H. Zhang, M. Gu, X. Jiang, J. Thompson, H. Cai, S. Paesani, R. Santagati, A. Laing, Y. Zhang, M. Yung, et al., *Nat. Commun.* **2021**, *12*, 457.
[51] Y. Gao, Y. Sun, I. Rebolledo-Salgado, R. Van Laer, V. Torres-company, S. Jochen, Data accompanying 'tightly-confined and long z-cut lithium niobate waveguide with ultralow-loss', **2025**.